Design of an All-Fiber Fabry-Perot Sensor for Strain Measurement in Radiative Environment

Tingting YANG[1], Zengling RAN[1*], Xiu HE[1], Lupeng GAN[1], Zhengxi HE[1,2], Jialiang ZHU[2], Peng HE[2], Zhuoyue LI[2], and Dong SUN[3]

[1]*Key Laboratory of Optical Fiber Sensing & Communications (Ministry of Education), University of Electronic Science and Technology of China, Chengdu 611731, China*

[2]*Science and Technology on Reactor System Design Technology Laboratory, Nuclear Power Institute of China, Chengdu 610213, China*

[3]*School of Information and Communication Engineering, University of Electronic Science and Technology of China, Chengdu 611731, China*

[*]Corresponding author: Zengling RAN E-mail: ranzl@126.com

Abstract: A length-matched micro Fabry-Perot (FP) interferometer is proposed for strain measurement under irradiation environment. Theoretical simulation shows that a well length-matched FP sensor can achieve a very low drift of the cavity length and strain sensitivity in irradiation environment. In experiment, such an FP cavity is realized by laser micromachining. It shows a low cavity length drift of −0.037 μm and a strain sensitivity deviation of 0.52%, respectively, under gamma irradiation. Meanwhile, the intensity of interference fringes is also stable. As a result, such a length-matched FP cavity is a very promising candidate for strain sensing in radiative environments.

Keywords: Gamma radiation; Fabry-Perot sensor; radiation-induced compaction; strain sensing

Citation: Tingting YANG, Zengling RAN, Xiu HE, Lupeng GAN, Zhengxi HE, Jialiang ZHU, *et al.*, "Design of an All-Fiber Fabry-Perot Sensor for Strain Mearement in Radiative Environment," *Photonic Sensors*, 2022, 12(4): 220418.

1. Introduction

The strain measurement of equipment in nuclear environments is vital for its safe operation. The Fabry-Perot (FP) sensor has been investigated extensively for strain measurement under radiative environment. F. Berghmans *et al.* [1] observed that the interferometer fringes of the capillary-based FP strain sensors were erased under irradiation. The cavity length changes of the capillary-based elongation FP sensors, caused by radiation-induced compaction (RIC) [2], have been reported [3–5]. After intense neutron-gamma radiation under high temperature, the cavity length of three surviving sensors drifted between 1 μm and 4 μm [5]. Recently, we reported pressure responses of an all-fiber air cavity FP sensors before and after gamma radiation [6]. These studies showed that radiation weakened the FP sensor's signal and degraded its measurement accuracy. Especially, RIC causes a drift in the cavity length, thereby introducing an obvious measurement error. To achieve accurate strain measurement in radiative environment, it is the key to eliminate the drift of the FP sensor and reduce signal attenuation.

Received: 21 September 2021 / Revised: 29 September 2021

DOI: 10.1007/s13320-022-0645-x
Article type: Regular

Additionally, considering that high temperature and irradiation usually exist at the same time, the strain sensor should have good high temperature resistance [7]. As a result, there is an urgent need to develop a method of designing a sensor, with low radiation sensitivity, low temperature sensitivity, and high operating temperature, for strain measurements in nuclear environments.

In this work, such a design method is proposed, for realizing an FP sensor that works stably in extreme radiation environment, based on a length-matched idea.

2. Design and analysis of the sensor

Figure 1 shows the FP cavity sensor, which is formed by splicing a single mode fiber (SMF) with a flat surface and a high-doped-germanium large diameter fiber (LDF) with a cone groove surface. The FP cavity consists of an air cavity and a gutter structure with lengths of L_0 and L_1, respectively.

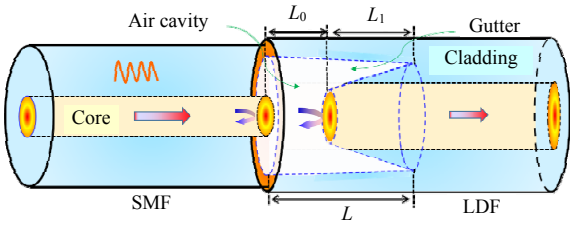

Fig. 1 Structure of the designed FP sensor head.

On one hand, compaction-induced air cavity length drift under irradiation causes a noticeable measurement error for an FP sensor. On the other hand, the strain sensitivity stability of the FP sensor is the key to achieve accurate strain measurement under irradiation. To realize an FP sensor suitable for radiative environment, we carry out a theoretical analysis on the compaction-induced cavity length drift and the strain sensitivity stability of the sensor after irradiation.

2.1 Analysis of radiation-induced cavity length drift

Under irradiation, RIC causes a decrease in the volume of silica [8]. The schematic diagram of the FP sensor is shown in Fig. 2. Before irradiation, the lengths of the FP cavity, air cavity, and gutter structure are set to L, L_0, and L_1, respectively. After irradiation, the changes in lengths of the FP cavity, air cavity, and gutter structure are set to ΔL, ΔL_0, and ΔL_1, respectively. From Fig. 2, the movement of the second reflective surface increases the length of L_0, denoted as ΔL_{0I}. The movement of the end faces to the cavity decrease the length of L_0, denoted as ΔL_{0D}. Then, the total change in length of L_0 is $\Delta L_0=\Delta L_{0I}+\Delta L_{0D}$. Actually, compaction causes the changes of L and L_1, which lead to a decrease and an increase in L_0, respectively. Deriving from $\Delta L_0=\Delta L-\Delta L_1$, we can get $\Delta L_0=\Delta L_{0I}+\Delta L_{0D}=\Delta L-\Delta L_1$, where $\Delta L>0$ and $\Delta L_1>0$, respectively. Assuming that the linear compaction coefficients of L_1 and L are k_{L1} and k_L, respectively, ΔL_0 can be expressed as

$$\Delta L_0 = \Delta L - \Delta L_1 = Lk_L - L_1 k_{L1}. \quad (1)$$

Compaction mainly depends on the fiber composition [8] and radiation source [9]. Thus, k_{L1} and k_L are different due to the difference of the fiber composition and radiation source. To show how L_0 varies with L_0/L_1 of the sensor, under different k_{L1} and k_L values, we calculate ΔL_0 for different cases using (1). The density change of vitreous silica has increased by 3% under fast neutron irradiation [10]. That gives 1% decrease in the length, if the compaction is isotropic. Under high neutron and gamma irradiation, the length decrease of radiation resistant fibers with different compositions corresponds to 0.24% – 0.34% of linear compaction [8]. Therefore, in calculation, it is assumed that k_{L1} and k_L are within the range of 0.2% – 1%.

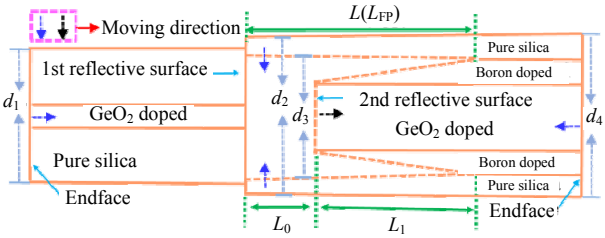

Fig. 2 Schematic diagram of radiation-induced compaction of the FP sensor.

Figure 3 shows ΔL_0 calculated for $k_{L1}<k_L$ [Fig. 3(a)], $k_{L1}=k_L$ [Fig. 3(b)], and $k_{L1}>k_L$ [Fig. 3(c)], respectively. From it, ΔL_0 depends on L_0/L_1 in any case, and the larger k_{L1} and k_L are, the larger ΔL_0 is. When $k_{L1}<k_L$, ΔL_0 increases as the difference between k_{L1} and k_L increases. In the cases where $k_{L1}<k_L$ and $k_{L1}=k_L$, ΔL_0 increases as L_0/L_1 increases. Accordingly, the use of fibers with excellent radiation resistance to make an FP sensor with a tiny L_0/L_1 can reduce the air cavity length drift. As shown in Fig. 3(c), when L_0/L_1 takes a specific value, ΔL_0 is zero. The reason is that, in this case, the changes of L and L_1 compensate each other under irradiation, namely, $\Delta L_1=\Delta L$, then, $\Delta L_0=k_L L-k_{L1}L_1=\Delta L-\Delta L=0$. Therefore, based on the calculation results of the case where $k_{L1}>k_L$, we propose a design method of an FP sensor, which is to select fibers with different core and cladding compositions to make the sensor, as well as the design of the ratio of L_0/L_1 to be at a suitable value. Namely, the cladding of the fiber has better radiation resistance than the core. As a result, the fiber with a highly Ge-doped core and a pure silica cladding, indicating that the linear compaction coefficient of the core is greater than that of the cladding, is selected for the production of the FP sensor. Theoretically, for the FP sensor made by this fiber, by controlling L_0/L_1, ΔL_0 can be reduced to zero under irradiation.

2.2 Stability analysis of strain sensitivity under radiation

For investigating the strain sensitivity stability, the FP sensor is fixed with a distance of L_T. A certain fixed strain of ε is applied. The strains of the FP cavity, SMF, and LDF are marked as ε_{FP}, ε_{SMF}, and ε_{LDF}, respectively.

Then, the total length of the FP strain sensor between the two fixed points is

$$L_T = L_{SMF} + L_{FP} + L_{LDF}. \quad (2)$$

The strains generated among the two fixed points of the FP strain sensor, the SMF, the FP cavity, and the LDF are respectively expressed as

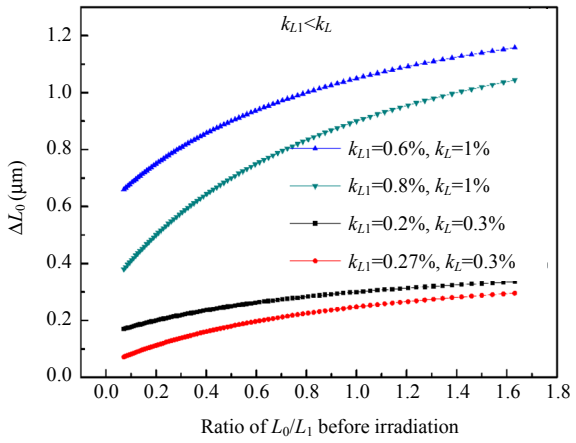

(a)

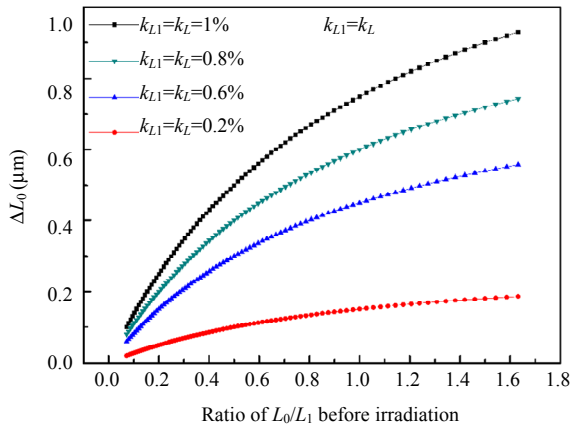

(b)

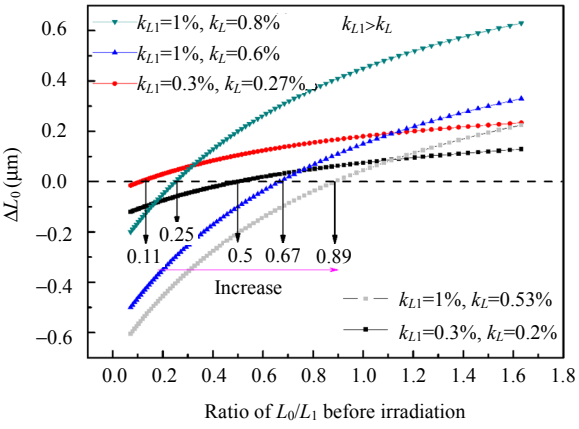

(c)

Fig. 3 Relationship between the calculated air cavity length drift (ΔL_0) of the sensor at different cases and the values of L_0/L_1 of the sensor: (a) $k_{L1}<k_L$, (b) $k_{L1}=k_L$, and (c) $k_{L1}>k_L$.

$$\varepsilon = \frac{\Delta L_T}{L_T},\ \varepsilon_{\mathrm{SMF}} = \frac{\Delta L_{\mathrm{SMF}}}{L_{\mathrm{SMF}}}$$
$$\varepsilon_{\mathrm{FP}} = \frac{\Delta L_{\mathrm{FP}}}{L_{\mathrm{FP}}},\ \varepsilon_{\mathrm{LDF}} = \frac{\Delta L_{\mathrm{LDF}}}{L_{\mathrm{LDF}}}. \tag{3}$$

When the force F is applied along the axial direction of the FP strain sensor, the strains produced by each part are different as the difference in their cross-sectional areas (S). According to $F = E\varepsilon S$, the following equation is obtained:

$$\begin{aligned}\varepsilon_{\mathrm{SMF}} E_{\mathrm{SMF}}(T) S_{\mathrm{SMF}}(T) &= \varepsilon_{\mathrm{FP}} E_{\mathrm{FP}}(T) S_{\mathrm{FP}}(T) \\ &= \varepsilon_{\mathrm{LDF}} E_{\mathrm{LDF}}(T) S_{\mathrm{LDF}}(T)\end{aligned} \tag{4}$$

where $E_{\mathrm{SMF}}(T)$, $E_{\mathrm{FP}}(T)$, and $E_{\mathrm{LDF}}(T)$ are the Young's modulus of the SMF, the cladding surround the air in the cavity, and the LDF, respectively, which are temperature dependent [11]. Correspondingly, $S_{\mathrm{SMF}}(T)$, $S_{\mathrm{FP}}(T)$, and $S_{\mathrm{LDF}}(T)$ are their cross-sectional areas. The FP cavity is made on the LDF, so its Young's modulus is the same as that of the LDF, denoted as $E_{\mathrm{FP}}(T)$.

Next, the strain applied to the FP strain sensor can be expressed as

$$\begin{aligned}\varepsilon &= \frac{L_{\mathrm{SMF}}\varepsilon_{\mathrm{SMF}} + L_{\mathrm{FP}}\varepsilon_{\mathrm{FP}} + L_{\mathrm{LDF}}\varepsilon_{\mathrm{LDF}}}{L_{\mathrm{SMF}} + L_{\mathrm{FP}} + L_{\mathrm{LDF}}} \\ &= \frac{L_{\mathrm{SMF}}\dfrac{\varepsilon_{\mathrm{FP}} S_{\mathrm{FP}}(T) E_{\mathrm{FP}}(T)}{S_{\mathrm{SMF}}(T) E_{\mathrm{SMF}}(T)} + L_{\mathrm{FP}}\varepsilon_{\mathrm{FP}} + L_{\mathrm{LDF}}\dfrac{\varepsilon_{\mathrm{FP}} S_{\mathrm{FP}}(T)}{S_{\mathrm{LDF}}(T)}}{L_{\mathrm{SMF}} + L_{\mathrm{FP}} + L_{\mathrm{LDF}}}.\end{aligned} \tag{5}$$

The relationship between the strains of the FP cavity and the FP strain sensor can be described as

$$\varepsilon_{\mathrm{FP}} = \frac{\varepsilon\left(L_{\mathrm{SMF}} + L_{\mathrm{FP}} + L_{\mathrm{LDF}}\right)}{L_{\mathrm{SMF}}\dfrac{E_{\mathrm{FP}}(T) S_{\mathrm{FP}}(T)}{E_{\mathrm{SMF}}(T) S_{\mathrm{SMF}}(T)} + L_{\mathrm{FP}} + L_{\mathrm{LDF}}\dfrac{S_{\mathrm{FP}}(T)}{S_{\mathrm{LDF}}(T)}}. \tag{6}$$

The relationship between the change in air cavity length and the FP strain sensor wavelength drift is as follows:

$$\frac{\Delta\lambda}{\lambda} = \frac{\Delta L_0}{L_0} = \frac{\Delta L_{\mathrm{FP}}}{L_0} = \frac{(L_0 + L_1)\varepsilon_{\mathrm{FP}}}{L_0} = (1 + L_1/L_0)\varepsilon_{\mathrm{FP}} \tag{7}$$

where $\Delta\lambda$ is the wavelength shift of the FP strain sensor under strain, and λ is the wavelength in vacuum. L_1 and L_0 are the initial lengths of the gutter and the air cavity, respectively.

Then, using (6) and (7), the strain sensitivity of the FP strain sensor is written as

$$\begin{aligned}k_\varepsilon &= \frac{\Delta\lambda}{\varepsilon} \\ &= \frac{(1 + L_1/L_0)\left(L_{\mathrm{SMF}} + L_0 + L_1 + L_{\mathrm{LDF}}\right)\lambda}{L_{\mathrm{SMF}}\dfrac{E_{\mathrm{FP}}(T) S_{\mathrm{FP}}(T)}{E_{\mathrm{SMF}}(T) S_{\mathrm{SMF}}(T)} + L_0 + L_1 + L_{\mathrm{LDF}}\dfrac{S_{\mathrm{FP}}(T)}{S_{\mathrm{LDF}}(T)}}.\end{aligned} \tag{8}$$

The diameter of the SMF, the outer and inner diameters of the FP cavity, and the diameter of the LDF are set to d_1, d_2, and d_3, and d_4, respectively, as shown in Fig. 2. Then, (8) can be expressed as

$$\begin{aligned}k_\varepsilon &= \frac{\Delta\lambda}{\varepsilon} \\ &= \frac{(1 + L_1/L_0)L_T\lambda}{L_{\mathrm{SMF}}\dfrac{E_{\mathrm{FP}}(T)(d_2^{\,2} - d_3^{\,2})}{E_{\mathrm{SMF}}(T) d_1^{\,2}} + L_0 + L_1 + L_{\mathrm{LDF}}\dfrac{(d_2^{\,2} - d_3^{\,2})}{d_4^{\,2}}}.\end{aligned} \tag{9}$$

According to (9), the strain sensitivity of the FP strain sensor depends on the Young's modulus and diameters of the SMF, the LDF, and the FP cavity, as well as the cavity length of the FP sensor. The factors that affect the strain sensitivity of the FP sensor under irradiation are as follows. Firstly, the Young's modulus of the silica increases by <0.5% under gamma irradiation [12]. Secondly, the diameter of the fiber changes under irradiation [13]. Thirdly, radiation causes a change in the FP cavity length. In comparison, the cavity length change is relatively obvious. Therefore, the strain sensitivity variation of the sensor is mainly caused by the change of L_0/L_1. Moreover, the Young's modulus and diameter of the fiber, which have tiny changes under irradiation, are not considered [12, 13]. Additionally, the SMF and the LDF are made of silica with the same Young's modulus. Besides, L_T does not change during the strain test before and after irradiation. Thus, (9) can be written as

$$k_\varepsilon = \frac{\Delta\lambda}{\varepsilon} = \frac{(1+L_1/L_0)L_T\lambda}{L_{\mathrm{SMF}}\dfrac{(d_2^{\,2}-d_3^{\,2})}{d_1^{\,2}} + L_0 + L_1 + L_{\mathrm{LDF}}\dfrac{(d_2^{\,2}-d_3^{\,2})}{d_4^{\,2}}} = k(1+L_1/L_0) \tag{10}$$

where

$$k = \frac{L_T\lambda}{\left(d_2^{\,2}-d_3^{\,2}\right)\left(L_{\mathrm{SMF}}/d_1^{\,2}+L_{\mathrm{LDF}}/d_4^{\,2}\right)+L_0+L_1}.$$

Assume that the strain sensitivities of the FP sensor before and after irradiation are $k_{\varepsilon b}$ and $k_{\varepsilon a}$, respectively. Then, the strain sensitivity deviation of the FP sensor is expressed as

$$\text{deviation} = \frac{k_{\varepsilon_b}-k_{\varepsilon_a}}{k_{\varepsilon_b}} = \frac{L_1/L_0\left[1-(1-k_{L1})/(1-k_L)\right]}{1+L_1/L_0} \tag{11}$$

where k_L and k_{L1} are linear compaction coefficients of L and L_1, respectively.

To provide a guidance for the sensor design, under different k_L and k_{L1} values, the strain sensitivity deviation of the sensor varying with the ratio of L_0/L_1 (before irradiation) of the FP strain sensor is calculated by (11), as shown in Fig. 4. From it, the strain sensitivity deviation is zero for the case of $k_{L1}=k_L$. The strain sensitivity deviation decreases with L_0/L_1 when $k_{L1}\neq k_L$. Moreover, when $k_{L1}>k_L$, the radiation-induced cavity length drift leads to a decrease in the strain sensitivity of the sensor. On the contrary, when $k_{L1}<k_L$, the radiation-induced cavity length drift leads to an increase in the strain sensitivity of the sensor. When $k_{L1}\neq k_L$, under the condition that L_0/L_1 is greater than 1, the strain sensitivity deviation changes little and tends to stabilize with an increase in L_0/L_1. Therefore, to achieve strain sensitivity stability of the sensor under irradiation, L_0/L_1 should not be less than 1. However, according to (10), the strain sensitivity of the sensor decreases with an increase in L_0/L_1. According to the theoretical analysis, for compromise between the strain sensitivity and stability under irradiation, the range of L_0/L_1 of the sensors should be designed to be between 0.6 and 1 with the maximum strain sensitivity deviation of 0.65%.

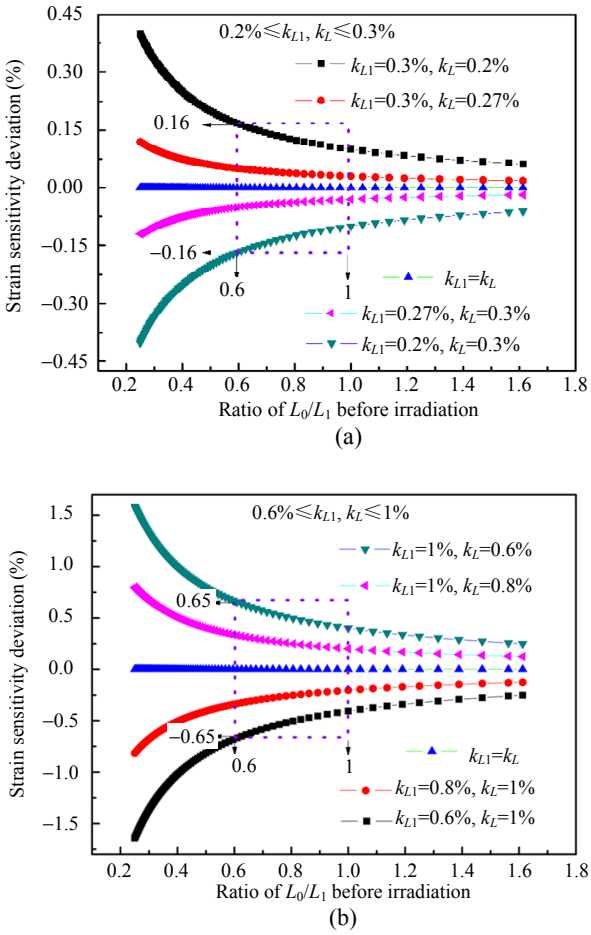

Fig. 4 Relationship between the calculated strain sensitivity deviations of the sensor at different cases and the values of L_0/L_1 of the sensor: (a) 0.2%≤k_{L1}, k_L≤0.3% and (b) 0.6%≤k_{L1}, k_L≤1%.

3. Sample preparation and experimental procedure

To verify the design method of the all-fiber FP sensor proposed above, as a proof of concept, seven FP sensors with different L_0/L_1 values are designed and fabricated. The production process of the sensor involves 4 steps as shown in Fig. 5. Firstly, a flat surface is formed by cleaving the LDF [Fig. 5(a)]. Secondly, a micro hole is drilled at the cleaved end face to form an air cavity via a circle mask [Mask I, Fig. 5(b)]. Thirdly, a gutter structure [Fig. 5(c)] is machined by using a ring-shaped mask (Mask II).

Fourthly, an SMF is spliced to the machined fiber to form an FP [Fig. 5(d)]. Additionally, the FP gauge length can be further adjusted by multi-discharging. The detailed production process of the sensor is described in [14]. The sensitivities of the sensor, with a very low temperature and strain cross sensitivities, and high temperature resistance, can be adjusted by controlling the cavity length [14]. The micrograph of the FP sensor is shown in Fig. 6. The bare FP samples with low temperature sensitivities are fixed on a stainless steel plate placed horizontally in gamma (1.25 MeV) radiative environment to ensure that they are exposed to the same dose rate of 1 kGy/h (SiO_2), and the accumulated dose is set to 279.483 kGy at 70 ℃. The performances of the FP sensor before and after irradiation are tested, including its air cavity length (L_0) variations, strain responses, and temperature responses.

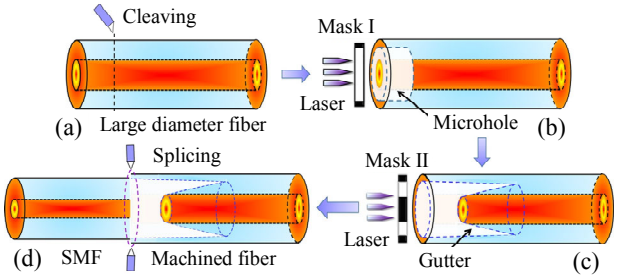

Fig. 5 Schematic diagram of the FP sensor production process: (a) cleaving the fiber, (b) micromachining to form a microhole, (c) micromachining to form a gutter, and (d) splicing to form an FP.

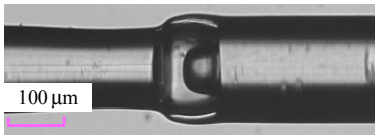

Fig. 6 Micrograph of the FP sensor.

4. Results and discussion

4.1 Air cavity length drift

After irradiation, visual inspection with a microscope reveals that the structure of the FP cavity of the seven sensors does not change. The micrographs of the sensor #4 before and after irradiation are shown in Fig. 7.

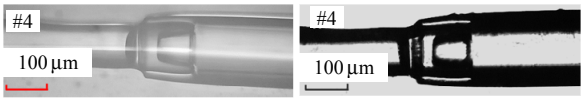

(a) (b)

Fig. 7 Micrographs of the sensor #4: (a) before irradiation and (b) after irradiation.

Seven FP sensors show an air cavity length drift of 0.037 μm to 5.383 μm, as shown in Table 1. The drift of 0.037 μm of the sensor #5 is two orders of magnitude smaller than the drift of 1 μm to 4 μm of the capillary-based elongation air cavity FP sensors [5]. From Table 1, it is found that ΔL_0 depends on L_0/L_1 of the sensor before irradiation, which is plotted in Fig. 8. From it, the air cavity length has a small drift when L_0/L_1 is between 0.63 and 0.81. And ΔL_0 is zero when L_0/L_1 takes a specific value within this range, as the analysis result of compaction-induced cavity length drifts. However, the shapes of the experimental curve and theoretically calculated curve are different. This is

Table 1 Air cavity length (L_0) drift of the seven FP sensors before and after irradiation.

No.	L_0/L_1 (before irradiation)	L_0 (μm)		Drift (μm)	Deviation (%)
		Before irradiation	After irradiation		
#1	1.200	39.398	34.015	5.383	13.60
#2	0.923	37.270	35.794	1.476	3.96
#3	0.920	39.682	39.074	0.608	1.53
#4	0.870	40.011	39.427	0.584	1.45
#5	0.810	43.545	43.582	−0.037	0.08
#6	0.631	39.409	39.501	−0.092	0.23
#7	0.450	36.069	36.683	−0.614	1.70

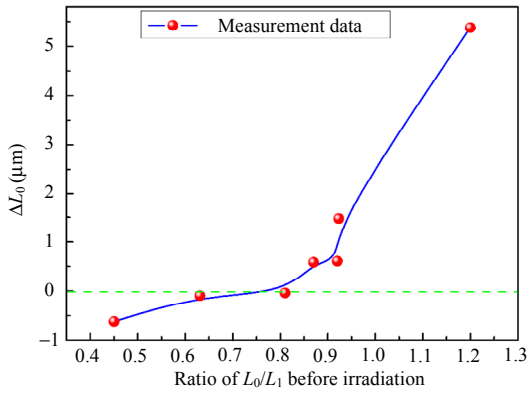

Fig. 8 Relationship between the air cavity length drifts of the seven sensors before and after irradiation and the values of L_0/L_1 of the seven sensors.

because, in fact, the compaction of the SMF and LDF affects the compaction of L. And, linear compaction coefficients of L and L_1 may be affected by the irregularity of the FP cavity structure. Nevertheless, the experimental results show that the design of sensors with the length-matched FP cavity can eliminate the radiation-induced cavity length drift. Additionally, the FP sensor could also be designed as a sensor for gamma detection by controlling the ratio of L_0/L_1.

4.2 Strain responses

The strain tests of the four FP sensors are carried out at room temperature before and after irradiation. The experimental setup is shown in Fig. 9, the FP sensor is fixed on two high-precision stages, and the force is applied along the axis of the fiber. The distance between the two fixed points is 100 cm. The test is repeated for three cycles to check the reproducibility of the sensors. Strain performances of these FP samples before and after irradiation are listed in Table 2. From it, compared with the results before irradiation, these samples present an increased or decreased strain sensitivity. The strain responses of the sensor #6 before and after radiation are presented as examples, and the inset is its spectra before and after irradiation, as shown in Fig. 10. It is observed that, after irradiation, the sensor #6 has the good spectral quality and its strain response has the good linearity. The strain sensitivity deviation of the FP sensor is discussed below.

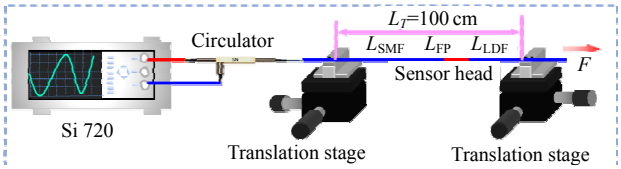

Fig. 9 Strain experimental setup.

Table 2 Comparison of strain responses of four FP sensors before and after irradiation.

Number	L_0/L_1 (before irradiation)	Strain sensitivity (pm/με)		Drift (pm/με)	Deviation (%)	Linearity	
		Before irradiation	After irradiation			Before irradiation	After irradiation
#1	1.200	3.06	3.19	−0.13	−4.24	0.9956	0.9969
#5	0.810	3.81	3.79	0.02	0.52	0.9960	0.9984
#6	0.631	4.91	4.71	0.20	4.07	0.9950	0.9969
#7	0.450	5.2	4.98	0.22	4.23	0.9956	0.9983

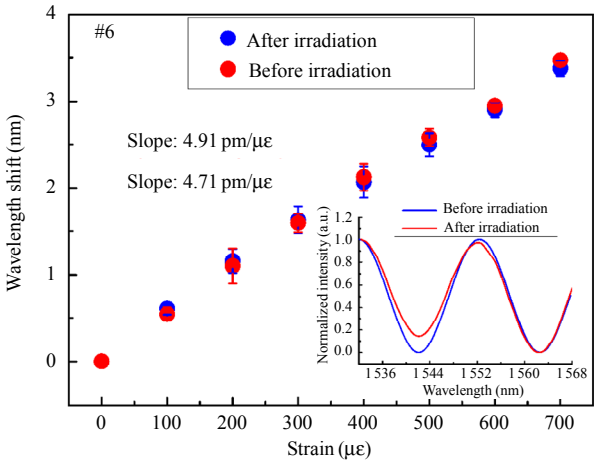

Fig. 10 Strain responses of the sensor #6 at room temperature before and after irradiation.

Using experimental data of the cavity length, the deviations of the strain sensitivities of the seven samples are calculated by (11). Figure 11 shows a comparison between calculated results and experimental results, by investigating the relationship between the strain sensitivities deviations and L_0/L_1 of the FP before irradiation. There is a difference between them, but the trend is consistent. We believe that the difference is mainly due to the fiber diameter change under irradiation. From Fig. 11, when L_0/L_1 ranges from 0.7 to 0.9, the strain sensitivity of the sensor has a small deviation and is independent of L_T. The sensor #5 has a minimum strain sensitivity deviation of 0.52%. This result is different from the theoretical analysis result

of the strain sensitivity deviation. This is also due to the influence of the compaction of the SMF and LDF and the irregularity of the FP cavity structure on k_{L1} and k_L. According to the experimental results, the strain sensitivity deviation of the FP sensor can be avoided or even eliminated by controlling the value of L_0/L_1.

4.3 Temperature responses

Compared with the results before irradiation, the samples have a larger temperature sensitivity, as shown in Table 3. Compared with the results of the FP temperature sensors reported in [15, 16], the temperature sensitivities of these samples have a larger variation. The changes in temperature sensitivities of the FP samples are greater than those of the strain sensitivities. Temperature responses of the sensor #6 before and after radiation are shown in Fig. 12.

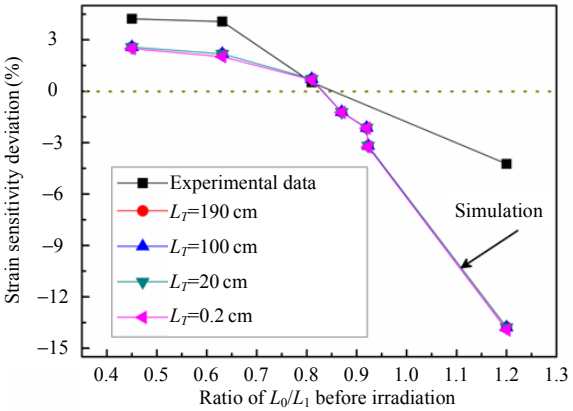

Fig. 11 Relationship between the strain sensitivity deviations of the sensor and the values of L_0/L_1 of the sensor before irradiation.

Table 3 Comparison of temperature responses of three FP samples before and after irradiation.

Number	L_0/L_1 (before irradiation)	Temperature sensitivity (pm/℃)		Drift (pm/℃)	Deviation (%)	Linearity	
		Before irradiation	After irradiation			Before irradiation	After irradiation
#3	0.920	−0.29	−0.32	0.03	−10	0.9870	0.9883
#6	0.631	−0.32	−0.50	0.18	−56	0.9971	0.9631
#7	0.450	−1.42	−1.91	0.49	−34	0.9969	0.9803

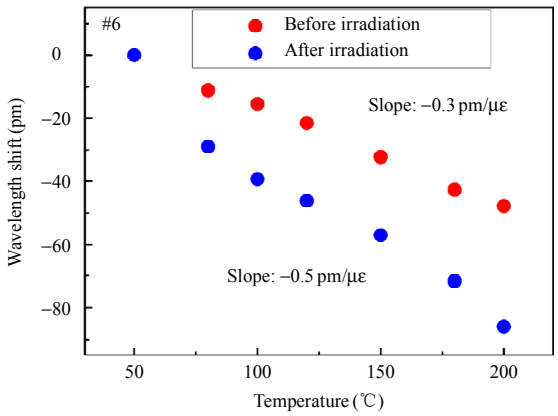

Fig. 12 Temperature response of the sensor #6 before and after irradiation.

Next, we discuss the temperature sensitivity drift factors of the FP sensor caused by irradiation.

The temperature sensitivity of the FP sensor can be written as

$$\frac{\Delta\varphi}{\Delta T}=\frac{4\pi}{\lambda_0}\left(n_0\frac{\Delta L_0}{\Delta T}+L_0\frac{\Delta n_0}{\Delta T}\right) \tag{12}$$

where n_0 is the initial refractive index of the air in the cavity, L_0 is the initial air cavity length, λ_0 is the wavelength in vacuum, $\Delta\varphi$ is the phase difference between the two beams, and ΔT is the change of temperature. According to $\Delta\varphi/2\pi = \Delta\lambda/\mathrm{FSR}$ and $\mathrm{FSR} = \lambda^2/2n_0L_0$, we can get $\Delta\lambda = \lambda^2\Delta\varphi/2\pi n_0L_0$. Here, FSR is the free spectral range of the reflection spectra. As a result, the temperature sensitivity of the FP sensors can be described as

$$\begin{aligned}k_T&=\frac{\Delta\lambda}{\Delta T}=\frac{\lambda_0}{n_0L_0}\left(n_0\frac{\Delta L_0}{\Delta T}+L_0\frac{\Delta n_0}{\Delta T}\right)\\&=\lambda_0\left(\frac{\Delta L_0}{L_0\Delta T}+\frac{\Delta n_0}{n_0\Delta T}\right).\end{aligned} \tag{13}$$

According to [14], the change of the air cavity length with temperature is expressed as

$$\Delta L_0 = \left[C_{\text{clad}} \left(L_0 + L_1 \right) - C_{\text{doped}} L_1 \right] \Delta T \qquad (14)$$

where C_{doped} and C_{clad} are thermal expansion coefficients of the doped cone region with a length of L_1 and the cladding of the LDF, respectively.

Then, (13) can be expressed as

$$k_T = \frac{\Delta\lambda}{\Delta T} = \lambda_0 \left[\frac{C_{\text{clad}} \left(L_0 / L_1 + 1 \right) - C_{\text{doped}}}{L_0 / L_1} + \delta \right] \qquad (15)$$

where $\delta = \Delta n_0 / (n_0 \Delta T)$ is the thermo-optical coefficient (TOC) of the air in cavity.

From (15), the temperature sensitivity of the FP sensor depends on the thermal expansion coefficient (TEC) of the LDF, the TOC of the air in the cavity, and the value of L_0/L_1. Therefore, the change in temperature sensitivities of the FP sensors after irradiation could be attributed to the following two factors. Firstly, radiation induces a change in the TEC of the LDF [12]. Secondly, after irradiation, the changes in L_0/L_1 of the sensors are different, which is the main reason for the different temperature sensitivity variations of these FP sensors. Besides, the effect of radiation on the TOC of the air in the cavity is currently unknown. Nonetheless, compared with strain sensitivities of the FP sensors, their temperature sensitivities are relatively low. Therefore, the influence of radiation on temperature characteristics of the FP sensors on their strain measurements can be neglected.

5. Conclusions

A method of designing a length-matched cavity FP sensor is proposed to resist the cavity length drift. The experimental results indicate that the sensor with a length-matched FP cavity exhibits the minimal cavity length drift of −0.037 μm and strain sensitivity deviation of 0.52% after gamma radiation (1 kGy/h, 279.483 kGy, and 70 ℃). Although large temperature sensitivity change is observed after irradiation, the analysis reveals that the influence of this change on the strain measurement can be neglected because the FP sensor has a relatively low temperature sensitivity. Using the sensor design method proposed in this work, an all-fiber extrinsic FP sensor with a length-matched FP has a great potential for the application in radiative environments.

Acknowledgment

This work was funded by the National Natural Science Foundation of China (Grant No. 51875091); the Study and Application of Full-Model Impact Dynamic Fretting Damage Test System in the Extreme Environment (Grant No. 51627806); Optical Fiber Sensing and Processing Prototype for Nuclear Field Key Parameter Measurement (Grant No. 191091); Data Acquisition and Post-Processing Software Development for Integrated Fiber Optic Sensors (Grant No. 190167); the State 111 Project (Grant No. B14039).

References

[1] F. Berghmans, A. F. Fernandez, B. Brichard, F. Vos, M. C. Decreton, A. I. Gusarov, *et al.*, “Radiation hardness of fiber optic sensors for monitoring and remote handling applications in nuclear environments,” in *Proceedings of SPIE – The International Society for Optical Engineering*, Boston, November 2–5, 1998, pp. 28–39.

[2] F. Piao, W. G. Oldham, and E. E. Haller, “The mechanism of radiation-induced compaction in vitreous silica,” *Journal of Non-Crystalline Solids*, 2000, 276(1–3): 61–71.

[3] G. Cheymol, J. F. Villard, A. Gusarov, and B. Brichard, “Fibre optic extensometer for high radiation and high temperature nuclear applications,” *IEEE Transactions on Nuclear Science*, 2011, 60(5): 3781–3784.

[4] G. Cheymol, C. Aubisse, B. Brichard, and M. Jacobs, "Fabry Perot sensor for in-pile nuclear reactor metrology," in *Optical Sensors 2008*, Strasbourg, 2008, pp. 700305.

[5] G. Cheymol, A. Gusarov, S. Gaillot, C. Destouches, and N. Caron, "Dimensional measurements under high radiation with optical fibre sensors based on white light interferometry–report on irradiation tests," *IEEE Transactions on Nuclear Science*, 2014, 61(4): 2075–2081.

[6] Z. Li, Z. Ran, X. Qing, Z. He, Y. Xiao, T. Yang, *et al.*, "Study of the sensing characteristics of irradiated fiber Bragg gratings and Fabry-Perot interferometers under gamma radiation," *Photonic Sensors*, 2022, 12(1): 91–98.

[7] J. R. Lee, Y. Chong, C. Y. Yun, and H. Sohn, "Design of fiber Bragg grating acoustic sensor for structural health monitoring of nuclear power plant," *Advanced Materials Research*, 2010, 123–125: 859–862.

[8] L. Remy, G. Cheymol, A. Gusarov, A. Morana, E. Marin, and S. Girard, "Compaction in optical fibres and fibre Bragg gratings under nuclear reactor high neutron and gamma fluence," *IEEE Transactions on Nuclear Science*, 2016, 63(4): 2317–2322.

[9] W. Primak and R. Kampwirth, "The radiation compaction of vitreous silica," *Journal of Applied Physics*, 1968, 39(12): 5651–5658.

[10] W. Primak, "Fast-neutron-induced changes in quartz and vitreous silica," *Physical Review*, 1958, 110(6): 1240–1254.

[11] S. Spinner and G. W. Cleek, "Temperature dependence of Young's modulus of vitreous germania and silica," *Journal of Applied Physics*, 1960, 31(8): 1407–1410.

[12] P. L. Higby, E. J. Friebele, C. M. Shaw, M. Rajaram, E. K. Graham, D. L. Kinser, *et al.*, "Radiation effects on the physical properties of low-expansion-coefficient glasses and ceramics," *Journal of the American Ceramic Society*, 1988, 71(9): 796–802.

[13] M. Bertolotti, A. Ferrari, F. Scudieri, and A. Serra, "Radii and refractive index changes in γ-irradiated optical fibers," *Radiation Effects*, 1979, 43(4–5): 177–180.

[14] T. Yang, Z. Ran, X. He, Z. Li, Z. Xie, Y. Wang, *et al.*, "Temperature-compensated multifunctional all-fiber sensors for precise strain/high-pressure measurement," *Journal of Lightwave Technology*, 2019, 37(18): 4634–4642.

[15] H. Liu, D. W. Miller, and J. Talnagi, "Gamma radiation resistant Fabry-Perot fiber optic sensors," *Review of Scientific Instruments*, 2002, 73(8): 3112–3118.

[16] H. Liu, J. Talnagi, and D. W. Miller, "Neutron radiation effects on Fabry-Perot fiber optic sensors," *Nuclear Instruments and Methods in Physics Research Section A: Accelerators, Spectrometers, Detectors and Associated Equipment*, 2003, 507(3): 691–702.